ARTICLE IN PRESS

Icarus xxx (xxxx) xxx

Contents lists available at ScienceDirect

Icarus

journal homepage: www.elsevier.com/locate/icarus

Research Paper

On the similarity of dust flows in the inner coma of comets

V.V. Zakharov [a,*], A. Rotundi [a,c], V. Della Corte [a,c], M. Fulle [d], S.L. Ivanovski [d], A.V. Rodionov [b], N.Y. Bykov [e]

[a] INAF – Istituto di Astrofisica e Planetologia Spaziali, Area Ricerca Tor Vergata, Via Fosso del Cavaliere 100, 00133 Rome, Italy
[b] RFNC–VNIIEF – Russian Federal Nuclear Center All–Russian Research Institute of Experimental Physics, Sarov, Nizhny Novgorod Region, 607188, Russia
[c] Università degli Studi di Napoli Parthenope, Dip. di Scienze e Tecnologie, CDN IC4, 80143 Naples, Italy
[d] INAF – Osservatorio Astronomico, Via Tiepolo 11, 34143, Trieste, Italy
[e] Peter the Great St.Petersburg Polytechnic University, Polytechnicheskaya, 29, St.-Petersburg, 195251, Russia

ARTICLE INFO

Keywords:
Comets: General – dust dynamics – numerical simulations

ABSTRACT

The atmosphere of a comet is formed by the sublimation, due to solar illumination, of its volatile component and the dust particles ejected from its nucleus and entrained by the gas flow. Contemporary dusty-gas coma models take into account numerous physical processes occurring in the coma and a complex geometry of the nucleus. For the description of the dusty-gas flow in the coma, such models introduce a large number of governing parameters characterizing physical properties and processes. The relative role of these processes is not easy to ascribe therefore a relevant inter-comparison of model results becomes difficult.

The present work introduces a set of universal, dimensionless parameters, which characterize the dust motion in the inner cometary coma. This approach allows one to: (i) reduce the number of parameters for analysis; (ii) reveal dust flows similarities; (iii) rescale the available numerical solutions. The present work demonstrates application of this approach to a realistic coma model.

Description of dust motion with dimensionless parameters allows us to make a parametric study for a broad range of conditions and to find simple analytic approximations (via a polynomial function) of the numerical results suitable for rough estimations of dust density in the coma.

1. Introduction

According to the current understanding, the nucleus of a comet consist of a mixture of ice, minerals and organics. The atmosphere of a comet is formed by the gas (produced by ice sublimation under solar illumination) and the dust particles ejected from the nucleus and entrained by the gas flow. At present there are a number of dusty-gas coma models, which take into account numerous physical processes and complex geometries, and use advanced methods of numerical simulation (e.g. Rodionov et al., 2002, Crifo et al., 2005, Zakharov et al., 2009, Tenishev et al., 2011, Fougere et al., 2013, Marschall et al., 2016). These models are able to predict with high resolution a complex spatial and temporal distribution of cometary atmosphere physical variables (density, velocity etc.), but require time-consuming numerical computations. For the description of the dusty-gas flow in the coma, such models introduce a large number of governing parameters characterizing physical properties and processes. Therefore the relative role of these processes is not easy to ascribe and relevant inter-comparison of model results becomes difficult.

The present work introduces a set of universal, dimensionless parameters characterizing the dust motion in the inner cometary coma. This approach allows to reduce the number of parameters for analysis, to reveal similarities of the dust flows and to rescale the available numerical solutions. Such approach was already applied in Zakharov et al. (2018) to an elementary model of the coma for the rough estimations of the dusty-gas flow properties and revealing of the asymptotic values (e.g. the dust terminal velocity, the time it takes to acquire it, and the distance at which it is acquired). The present work demonstrates how this approach can be applied to a more general coma models.

The contemporary state of space research allows us to undertake special missions into the inner atmosphere of a comet (coma) and/or perform flight-by close to the nucleus. For example, the future mission "Comet Interceptor" (see Snodgrass and Jones, 2019) of the European Space Agency assumes penetration into the innermost coma of a dynamically new comet. For the spacecraft and payload safety and to ensure instruments operation efficiency, predicting cometary coma parameters is critical. In fact, this allows to foresee the dust hazard,

* Corresponding author.
E-mail address: vladimir.zakharov@inaf.it (V.V. Zakharov).

https://doi.org/10.1016/j.icarus.2021.114476
Received 16 September 2020; Received in revised form 10 April 2021; Accepted 14 April 2021
Available online 18 April 2021
0019-1035/

i.e. the main risk. Collisions with dust involve both risks of contamination with further loss/damage of instruments or the whole spacecraft, and risks of collisional destruction of the spacecraft.

Dust motion described by dimensionless parameters allows a parametric study for a broad range of conditions. In addition, since with such approach it is possible to find a simple analytic approximation (via a polynomial function) of the results of numerical simulations, it allows to make rough dust density estimations in the coma. In the early stages of operational planning of a cometary mission, the assessment of coma parameters do not have to be very precise numerically, but should keep the main trends of the processes in the coma. Therefore, we use a simplified model of the gas environment (Zakharov et al., 2021), which is based on integral characteristics of the coma and asymptotic behavior of gas motion.

2. The model

We assume that the dusty-gas coma is formed by the gas sublimating from the nucleus (from the surface and/or from the interior) and solid particles (mineral or/and icy) released from the nucleus with zero initial velocity and entrained by the gas flow. It is assumed that the dusty-gas flow is coupled in one way only – the gas drags the dust (i.e. the presence of dust in the coma does not affect the gas motion), and that the dust particles do not collide with each other (the assumption of no feedback on the gas for most comae was articulated in Tenishev et al., 2011). The dust particles are assumed to be isothermal, spherical and internally homogeneous with invariable size and mass. To compute the dust distributions at distances comparable to the nucleus size, it is convenient to adopt a frame attached to the nucleus (i.e., rotating and translating with it): the inertia forces associated with the nucleus rotation and translation must be taken into consideration. Under these assumptions, dust particle motion is governed by the equations (Crifo et al., 2005):

$$m_d \frac{d\vec{v}_d}{dt} = \vec{F}_A + \vec{F}_G + \vec{F}_S + \vec{F}_I \tag{1}$$

$$\frac{d\vec{r}}{dt} = \vec{v}_d \tag{2}$$

where t is the time, $\vec{r}$, $\vec{v}_d$ are the particle radius and velocity vectors, and m_d particle mass, $\vec{F}_A$ is the aerodynamic force, $\vec{F}_G$ is the nucleus gravity force, $\vec{F}_S$ is the solar force, and $\vec{F}_I$ is the inertia force.

For isothermal, spherical and internally homogeneous nonsublimating grains, the aerodynamic force degenerates to a drag force:

$$\vec{F}_A = \frac{(\vec{v}_g - \vec{v}_d)^2}{2} \frac{(\vec{v}_g - \vec{v}_d)}{|\vec{v}_g - \vec{v}_d|} \rho_g \sigma_d C_D(s, \frac{T_d}{T_g}) \tag{3}$$

where σ_d and T_d are the particle cross-section and temperature, ρ_g, v_g, T_g are the gas density, velocity and temperature, C_D is the drag coefficient. For a spherical particle $\sigma_d = \pi a^2$ and $m_d = \frac{4}{3}\pi a^3 \rho_d$, where a is the particle radius and ρ_d is the particle specific density. If the particle size a is much smaller than the mean free path of the gas molecules (typical case in the coma), the drag coefficient C_D can be estimated by the "free-molecular" expression for a spherical particle (see Bird, 1994):

$$C_D\left(s, \frac{T_d}{T_g}\right) = \frac{2s^2+1}{s^3\sqrt{\pi}} \exp(-s^2) + \frac{4s^4+4s^2-1}{2s^4} \mathrm{erf}(s) + \frac{2\sqrt{\pi}}{3s}\sqrt{\frac{T_d}{T_g}} \tag{4}$$

where $s = |\vec{v}_g - \vec{v}_d|/\sqrt{2T_g k_B/m_g}$ is a speed ratio, m_g is the mass of the molecule, k_B is the Boltzmann constant.

The nucleus gravitational force $\vec{F}_G$ is:

$$\vec{F}_G = m_d \vec{g} \tag{5}$$

where $\vec{g}$ is the gravitational acceleration in the field of the nucleus. For the spherical nucleus $\vec{g} = -GM_N\vec{r}/|r^3|$ where G is the gravitational constant, M_N is the mass of the nucleus.

The solar force $\vec{F}_S$ is given, for spherical grains, by:

$$\vec{F}_S = \left(\frac{GM_\odot m_d}{r_{h,d}^2 r_\oplus^2} - \sigma_d \frac{Q_{ef} c_\odot \xi(\vec{r})}{c r_{h,d}^2}\right)\vec{i}_{\odot,d} \tag{6}$$

where $M_\odot$ is the mass of the Sun, Q_{ef} is the radiation pressure efficiency, c is the velocity of light, $c_\odot$ is the solar energy flux at 1AU, r_h is the heliocentric distance of the nucleus (in AU), $r_{h,d}$ is the dust particle heliocentric distance (in AU), $r_\oplus = 1.496 \cdot 10^{11}$ m is the Earth orbit semimajor axis, $\vec{i}_{\odot,d}$ is the unit vector directed from the dust particle to the Sun, and $\xi(\vec{r}) = 0$ if $\vec{r}$ is inside the shadow, and $\xi(\vec{r}) = 1$ if $\vec{r}$ is in sunlight.

In the adopted nucleus-attached frame, the inertia force $\vec{F}_I$ is given (Landau and Lifshitz, 1976) by:

$$\vec{F}_I = m_d\left[\frac{GM_\odot}{r_h^2 r_\oplus^2}\vec{i}_{\odot,n} + \vec{r}\times\frac{d\vec{\Omega}}{dt} + \vec{\Omega}\times(\vec{r}\times\vec{\Omega}) + 2\vec{v}_d\times\vec{\Omega}\right] \tag{7}$$

where $\vec{i}_{\odot,n}$ is the unit vector from the nucleus center-of-mass to the Sun and $\vec{\Omega}$ is the nucleus angular speed.

Introducing the parameter β (Fulle, 2004)

$$\beta = \frac{3c_\odot r_\oplus^2}{4GM_\odot c}\frac{Q_{ef}}{\rho_d a} = 5.7\cdot 10^{-4}\frac{Q_{ef}}{\rho_d a} \tag{8}$$

we may rewrite the sum $\vec{F}_S + \vec{F}_I$ as follows:

$$\vec{F}_S + \vec{F}_I = \frac{m_d GM_\odot}{r_h^2 r_\oplus^2}\left[(1-\beta\xi(\vec{r}))\frac{r_h^2}{r_{h,d}^2}\vec{i}_{\odot,d} - \vec{i}_{\odot,n}\right] + m_d\left(\vec{r}\times\frac{d\vec{\Omega}}{dt} + \vec{\Omega}\times(\vec{r}\times\vec{\Omega}) + 2\vec{v}_d\times\vec{\Omega}\right) \tag{9}$$

Following Zakharov et al. (2018) we introduce the following dimensionless variables: $\theta = T_d/T_s$, $\tilde{v}_g = v_g/v_g^{max}$, $\tilde{v}_d = v_d/v_g^{max}$, $\tilde{r} = r/R_N$, $\tilde{t} = t/\Delta t$, $\tau = T_d/T_g$, $\tilde{\rho}_g = \rho_g/\rho_s$, $\tilde{\Omega} = \Omega/\Omega_N$. Here $v_g^{max} = \sqrt{\gamma\frac{\gamma+1}{\gamma-1}\frac{k_b}{m_g}T_s}$ is the theoretical maximum velocity of gas expansion, ρ_s and T_s are the gas density and temperature on the sonic surface (i.e. where the gas velocity is equal the local sound velocity $\sqrt{\gamma k_B T_g/m_g}$) at the subsolar point, γ is the specific heat ratio, R_N is the characteristic linear scale (e.g. the radius of the nucleus), Ω_N is the characteristic angular velocity of the nucleus, and $\Delta t = R_N/v_g^{max}$. In addition, we introduce $\tilde{g}$ via normalizing g on GM_N/R_N^2 (therefore, in the case of a spherical nucleus $\tilde{g} = -\vec{r}/|\vec{r}^3|$).

In most models of the nucleus activity (sublimation from the surface or from inside of the surface layer), the gas molecules leave the surface with the velocity distribution function close to half-Maxwellian. Therefore, a non-equilibrium near-surface layer (Knudsen layer), where initially non-equilibrium flow (due to the boundary conditions) relaxes to an equilibrium state, forms close to the surface. The size of this layer depends on the gas production of the surface and may vary considerably. When the Knudsen layer is thin (i.e. strong gas production) the surface temperature T_n and the gas temperature on the sonic surface T_s can be related (see Crifo et al., 2002):

$$\sqrt{\frac{T_s}{T_n}} = \sqrt{1+\left(\sqrt{\frac{\gamma\pi}{8}}\frac{\gamma-1}{\gamma+1}\right)^2} - \sqrt{\frac{\gamma\pi}{8}}\frac{\gamma-1}{\gamma+1}. \tag{10}$$

For $\gamma = 1.33$ (i.e. for vibrationally relaxed H_2O) the ratio of temperatures is $T_s/T_n = 0.8152$. The gas density on the sonic surface ρ_s can be estimated as: $\rho_s = q/\sqrt{\gamma k_b T_s/m_g}$, where q is the local gas production rate [kg m^{-2}s^{-1}] of the surface in subsolar point.

Using the dimensionless variables, the Eqs. (1) and (2) can be rewritten as:

$$\frac{d\vec{v}_d}{d\tilde{t}} = \tilde{\rho}_g(\vec{v}_g - \vec{v}_d)^2\frac{\vec{v}_g - \vec{v}_d}{|\vec{v}_g - \vec{v}_d|}C_D(s,\tau)\ \mathrm{Iv} + \mathrm{Fu}\ \vec{g} + \frac{R_N GM_\odot}{(v_g^{max})^2 r_h^2 r_\oplus^2}\left[(1-\beta\xi(\vec{r}))\frac{r_h^2}{r_{h,d}^2}\vec{i}_{\odot,d} - \vec{i}_{\odot,n}\right] + \tag{11}$$

$$\left(\mathrm{Cr}\ \vec{\tilde{r}}\times\frac{d\vec{\tilde{\Omega}}}{d\tilde{t}}+\mathrm{Cr}^2\ \vec{\tilde{\Omega}}\times(\vec{\tilde{r}}\times\vec{\tilde{\Omega}})+\mathrm{Cr}\ 2\vec{\tilde{v}}_d\times\vec{\tilde{\Omega}}\right)$$

$$\frac{d\vec{\tilde{r}}}{d\tilde{t}}=\vec{\tilde{v}}_d \tag{12}$$

If the linear size of computational domain is much smaller than r_h, then $r_h\simeq r_{h,d}$ and $\vec{i}_{\odot,d}\simeq\vec{i}_{\odot,n}$. In this case Eq. (11) may be rewritten as:

$$\frac{d\vec{\tilde{v}}_d}{d\tilde{t}}=\tilde{\rho}_g(\vec{\tilde{v}}_g-\vec{\tilde{v}}_d)^2\frac{\vec{\tilde{v}}_g-\vec{\tilde{v}}_d}{|\vec{\tilde{v}}_g-\vec{\tilde{v}}_d|}C_D(s,\tau)\ \mathrm{Iv}+\mathrm{Fu}\ \vec{\tilde{g}}-\mathrm{Ro}\ \xi(\vec{\tilde{r}})\vec{i}_{\odot,n}+\left(\mathrm{Cr}\ \vec{\tilde{r}}\times\frac{d\vec{\tilde{\Omega}}}{d\tilde{t}}+\mathrm{Cr}^2\ \vec{\tilde{\Omega}}\times(\vec{\tilde{r}}\times\vec{\tilde{\Omega}})+\mathrm{Cr}\ 2\vec{\tilde{v}}_d\times\vec{\tilde{\Omega}}\right). \tag{13}$$

As a consequence of this assumption, this paper neglects the solar tidal forces that affect significantly the dust motion out of the acceleration zone over long times (weeks and longer). In addition, for particles equal and larger than mm-sized these effects are important also just outside the dust acceleration zone. The rigorous computation in the heliocentric reference frame of the dust motion out of cometary Hill's sphere can be found in Fulle et al. (1995).

The Eqs. (11) and (13) contain four dimensionless parameters:

$$\mathrm{Iv}=\frac{1}{2}\frac{\rho_s\sigma_d R_N}{m_d}=\frac{3}{8}\frac{\rho_s R_N}{a\varrho_d}=\frac{3Q_g^{sph}m_g}{32R_N a\varrho_d\pi\sqrt{T_s\gamma k_B/m_g}} \tag{14}$$

and

$$\mathrm{Fu}=\frac{GM_N}{R_N}\frac{1}{(v_g^{max})^2} \tag{15}$$

and

$$\mathrm{Ro}=\frac{1}{m_d(v_g^{max})^2}R_N\frac{\sigma_d Q_{ef}c_\odot}{cr_h^2} \tag{16}$$

and

$$\mathrm{Cr}=\frac{R_N\Omega_N}{v_g^{max}}=\Delta t\Omega_N. \tag{17}$$

Here Q_g^{sph} is the total gas production rate [s^{-1}] of a spherical nucleus of radius R_N with the local gas production uniform over the surface and equal the gas production in subsolar point. The dimensionless parameters Iv, Fu, Ro for the first time were introduced in Zakharov et al. (2018).

We note that the theoretical maximum velocity of gas expansion could be expressed also in terms of a stagnation temperature T_0 and a heat capacity C_p as $v_g^{max}=\sqrt{2C_pT_0}$. In this way the gas velocity on the sonic surface is $v_s=\sqrt{2C_pT_0}\sqrt{\frac{\gamma-1}{\gamma+1}}$ and the local gas production is $q=\rho_s v_s$. Therefore we can rewrite Iv as:

$$\mathrm{Iv}=\sqrt{\frac{\gamma+1}{2(\gamma-1)}}\frac{3qR_N}{8\sqrt{C_pT_0}a\varrho_d}. \tag{18}$$

The second term in this equation is the reciprocal of a dimensionless similarity parameter characterizing the ability of a dust particle to adjust to the local gas velocity introduced in Probstein (1969).

As can be seen these parameters have the following meaning:

1. Iv represents the ratio of the gas mass present in a flow tube, with the cross section of the particle and a characteristic length R_N, to the particle mass. This parameter characterizes the efficiency of entrainment of the particle within the gas flow (i.e. the ability of a dust particle to adjust to the gas velocity);
2. Fu represents the ratio of the comet surface gravitational potential to the flow thermodynamic potential (enthalpy, C_pT_0). This parameter characterizes the efficiency of gravitational attraction;
3. Ro represents the ratio of the specific work done by the solar pressure force on the characteristic length R_N to the flow thermodynamic potential. This parameter characterizes the contribution of solar radiation pressure;
4. Cr characterizes the influence of the nucleus (and the nucleus attached frame) rotation (via the centrifugal and Coriolis forces);

In order to define Iv, Fu, Ro, Cr it is necessary to know: m_g, γ, ρ_s, T_s, R_N, M_N, Ω_N, a and ϱ_d (or σ_d and m_d), Q_{ef} and r_h.

The condition that the particle could be lifted from the surface with the local normal vector $\vec{n}$ is:

$$\mathrm{Iv}\ \tilde{\rho}_g\tilde{v}_g^2C_D(s,\tau)\frac{\vec{\tilde{v}}_g}{|\vec{\tilde{v}}_g|}\cdot\vec{n}>\mathrm{Ro}\ \xi(\vec{\tilde{r}})\vec{i}_{\odot,n}\cdot\vec{n}-\left(\mathrm{Fu}\ \vec{\tilde{g}}+\mathrm{Cr}\ \vec{\tilde{r}}\times\frac{d\vec{\tilde{\Omega}}}{d\tilde{t}}+\mathrm{Cr}^2\ \vec{\tilde{\Omega}}\times(\vec{\tilde{r}}\times\vec{\tilde{\Omega}})\right)\cdot\vec{n}. \tag{19}$$

Assuming the Knudsen layer infinitely thin, steady rotation of the nucleus with $\vec{\tilde{\Omega}}\perp\vec{i}_{\odot,n}$, the condition that the particle could be lifted from the surface of a spherical nucleus at subsolar point is:

$$\mathrm{Iv}\ \frac{\gamma-1}{\gamma+1}C_D(\sqrt{\gamma/2},\theta)>\mathrm{Ro}+\mathrm{Fu}-\mathrm{Cr}^2. \tag{20}$$

For $0\le\mathrm{Ro}-\mathrm{Cr}^2\ll\mathrm{Fu}$, $\theta=1$, $\gamma=1.33$ this condition is: $0.794\ \mathrm{Iv}>\mathrm{Fu}$. The maximum liftable size a_{max} is:

$$a_{max}=\frac{3C_D(\sqrt{\gamma/2},\theta)R_N^2\rho_sT_s\gamma k_B/m_g}{8\varrho_dM_NG}=\frac{3Q_g^{sph}m_gC_D(\sqrt{\gamma/2},\theta)\sqrt{T_s\gamma k_B/m_g}}{32\varrho_d\pi M_NG} \tag{21}$$

and $a_{max}=0.579\cdot10^{-12}\rho_sT_sR_N^2/(\varrho_dM_Nm_g)=1.075\cdot10^{-2}Q_g^{sph}\sqrt{T_sm_g}/(\varrho_dM_N)$ for $\theta=1$, $\gamma=1.33$. This definition of a_{max} is based on a canonic model of particle ejection proposed by Whipple (1950) and refined in Gombosi et al. (1986), Crifo and Rodionov (1997), Crifo et al. (2005). This model assumes the absence of any cohesive forces restraining particle emission and a uniform outflow of gas at sonic velocity in a direction opposite to the force of gravitational attraction by the nucleus.

The local production rate q_d of dust particles with size a is related to the local gas proportion rate q via the dust-to-gas mass flux ratio $\chi(a)$:

$$q_d(a)=q\chi(a). \tag{22}$$

3. Results

In order to illustrate how the approach with dimensionless parameters can be used, we consider the dusty-gas coma in a simplified model of a cometary nucleus and coma. It is assumed that the nucleus is spherical, homogeneous and the local gas production, q, follows the cosine power law of solar zenith angle z_{sun} on the sunlit side and it is uniform on the night side:

$$q(z_{sun})\propto\max\{\cos^\alpha(z_{sun}),a_n\}; \tag{23}$$

where $a_n=q(180°)/q(0°)$ is the relative activity of the night side. It is assumed that the Knudsen layer is thin and the gas achieves the sonic velocity in the immediate vicinity of the surface. The gas distribution in the coma is taken from Zakharov et al. (2021). Fig. 1 shows the distributions of gas density and velocity for the gas production with $\alpha=1$ and for two cases $a_n=1.0$ (i.e. the spherical expansion) and $a_n=0.01$.

We note that our description of the dust dynamics, based on the dimensionless parameters, does not depend on the model used for the gas flow description (Euler, Navier–Stokes, DSMC etc.). Since the Euler description does not include viscous dissipation (i.e. it does not depend on the rarefaction), the gas distributions based on it may be re-scaled for different production rate and/or the nucleus size. For the gas distribution obtained with a model that includes the viscous dissipation (and if its effect is sizeable), the similarity of the dust dynamics holds only within this gas distribution.

For the numerical simulations of dust distribution in the coma we use the so-called Dust Monte-Carlo method exposed in details in Crifo et al. (2005).

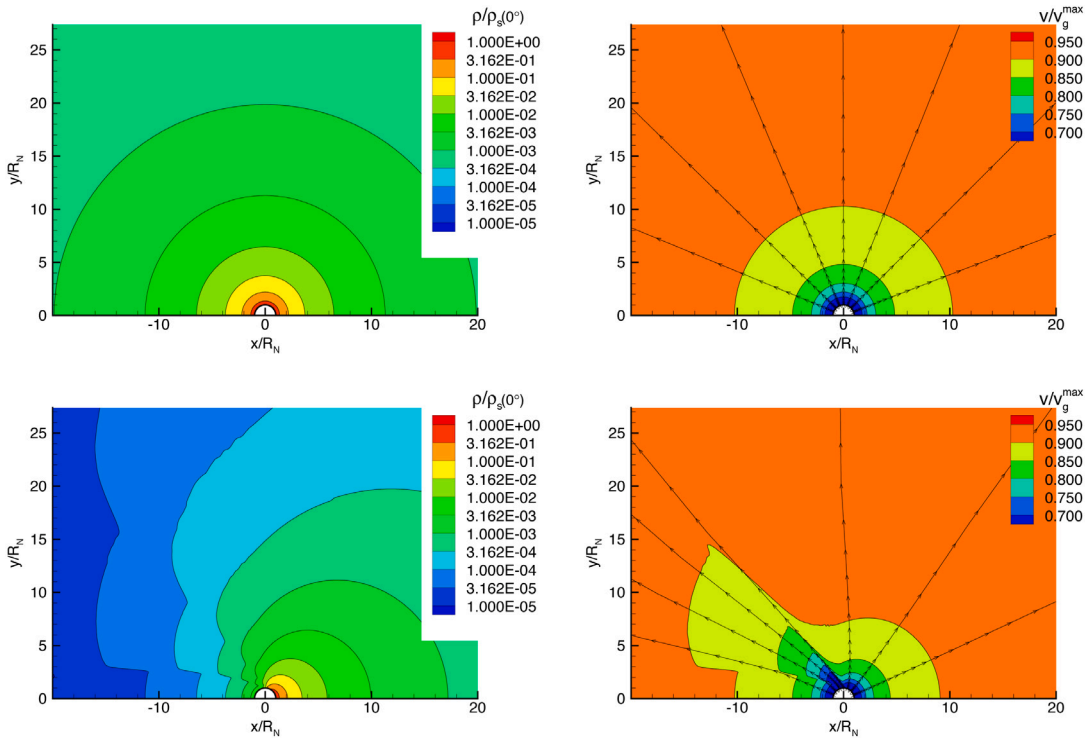

Fig. 1. Distribution of dimensionless gas density $\tilde{\rho}_g = \rho_g/\rho_s(0^\circ)$ (left) and velocity $\tilde{v}_g = v_g/v_g^{max}$ (right) from spherical nucleus with the surface flux uniformly distributed over the surface ($a_n = 1.0$) (top), and the surface flux proportional to $\cos(z_{sun})$ and $a_n = 0.01$ (bottom). The thin black lines with arrows show the gas flow lines.

Table 1
Parameters of the solutions.

parameter	case1	case2	case3
a_n	0.01	0.01	0.01
r_h [AU]	1.0	1.0	1.0
R_N [m]	10^3	10^3	10^4
M_N [kg]	10^{13}	10^{13}	10^{14}
T_N [K]	206.6	206.6	206.6
Q_g^{sph} [s^{-1}]	$7.3 \cdot 10^{27}$	$7.3 \cdot 10^{27}$	$7.3 \cdot 10^{29}$
ρ_s	$5.5 \cdot 10^{-8}$	$5.5 \cdot 10^{-8}$	$5.5 \cdot 10^{-8}$
a [m]	10^{-4}	10^{-3}	10^{-3}
ϱ_d [kg/m^3]	800.0	80.0	800.0
Q_{ef}	1.0	1.0	1.0
T_d [K]	206.6	206.6	206.6
Iv	$2.6 \cdot 10^{-4}$	$2.6 \cdot 10^{-4}$	$2.6 \cdot 10^{-4}$
Fu	$9.2 \cdot 10^{-7}$	$9.2 \cdot 10^{-7}$	$9.2 \cdot 10^{-7}$
Ro	$5.9 \cdot 10^{-8}$	$5.9 \cdot 10^{-8}$	$5.9 \cdot 10^{-8}$

In further examples of the dust density distribution it is assumed that $\chi(a) = 1.0$. This value may seem too high for the assumption of no feedback from dust to gas. We draw attention to the fact that under the assumption that dust particles do not collide with each other, χ is just a linear factor in the expression of density. Therefore, the dust density for the desirable χ can be obtained by simple multiplication of this χ and the density computed for $\chi = 1$. Also, for simplicity, we assume that Cr = 0 and $\theta = 1$.

3.1. Similarity of solutions with the same Iv, Fu, Ro

Fig. 2 shows the distributions of dimensionless dust density $\tilde{\rho}_d = \rho_d/\rho_s$ and dimensionless dust velocity $\tilde{v}_d = v_d/v_g^{max}$ for case 1–3 from Table 1. Though the parameters of the dust particles and/or the nucleus have different values, cases 1–3 have the same Iv, Fu, Ro. It is easy to notice that the cases with the same gas distribution are identical (black isocontours accurately follow the color transitions and the white dashed isocontours overlap the black ones). This example demonstrates that the dust distribution obtained for one set of physical parameters can be rescaled for another set of physical parameters (e.g. mass and/or size of the dust or of the nucleus) keeping the same set of dimensionless parameters.

3.2. Angular distribution of the dust density

Fig. 3 shows two examples of the spatial distribution of dimensionless dust density $\tilde{\rho}_d = \rho_d/\rho_s$ and dimensionless dust velocity $\tilde{v}_d = v_d/v_g^{max}$. White lines show the trajectories of dust particles in these plots. An example with Iv = 100, Fu = 10^{-9}, Ro = 10^{-7} corresponds the case when Iv is much greater than Fu and Ro i.e. the gas drag is the dominant factor in the dust motion in the entire region of simulation ($r/R_N \leq 1000$). In this case, at the distances $r/R_N > 10$ the dust motion is close to radial with practically constant velocity in the radial direction.

The example with Iv = 10^{-2}, Fu = 10^{-9}, Ro = 10^{-5} corresponds to the case with Iv still greater than Fu and Ro, but since the gas drag (and nucleus gravity as well) decreases with the distance to the nucleus, while the solar pressure force remains constant, at large distances from the nucleus, the solar pressure force becomes dominant and turns dust away from the Sun.

Figs. 4–7 show the angular distribution of the normalized dust density $\rho_d/\rho_s \cdot (r/R_N)^2$ at $r/R_N = 100$ and 1000 for the gas production with $\alpha = 1$–3, and $a_n = 1.0$ and 0.01 (see Eq. (23)) in the range of parameters: $10^{-3} \leq$ Iv $\leq 10^2$, $10^{-9} \leq$ Fu $\leq 10^{-4}$ and $10^{-7} \leq$ Ro $\leq 10^{-2}$.

The solar radiation pressure force (characterized by Ro) decelerates the dust motion in the sunward direction until it turns away from the Sun (qualitatively similarly to the low left panel of Fig. 3). In the vicinity of the *turning surface* (from where the dust turns away from the Sun) there is a strong increase of dust density. The position of this

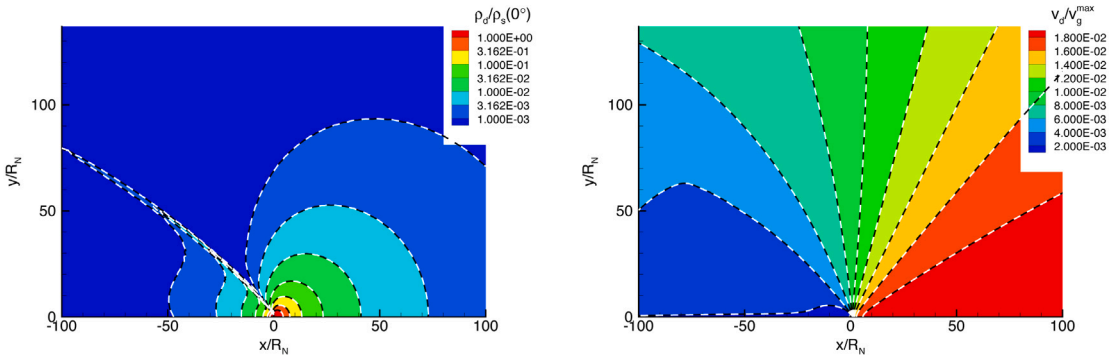

Fig. 2. Distribution of dimensionless dust density $\tilde{\rho}_d = \rho_d/\rho_s(0°)$ (left) and velocity $\tilde{v}_d = v_d/v_g^{max}$ (right) for Iv = $2.6 \cdot 10^{-4}$, Fu = $9.2 \cdot 10^{-7}$, Ro = $5.9 \cdot 10^{-8}$. Gas distribution corresponds to the expansion from spherical source with surface flux proportional to the cosine of solar zenith angle and $a_n = 0.01$. Case 1 is shown by color coding, case 2 is shown by black isocontours, and case 3 is shown by white dashed isocontours.

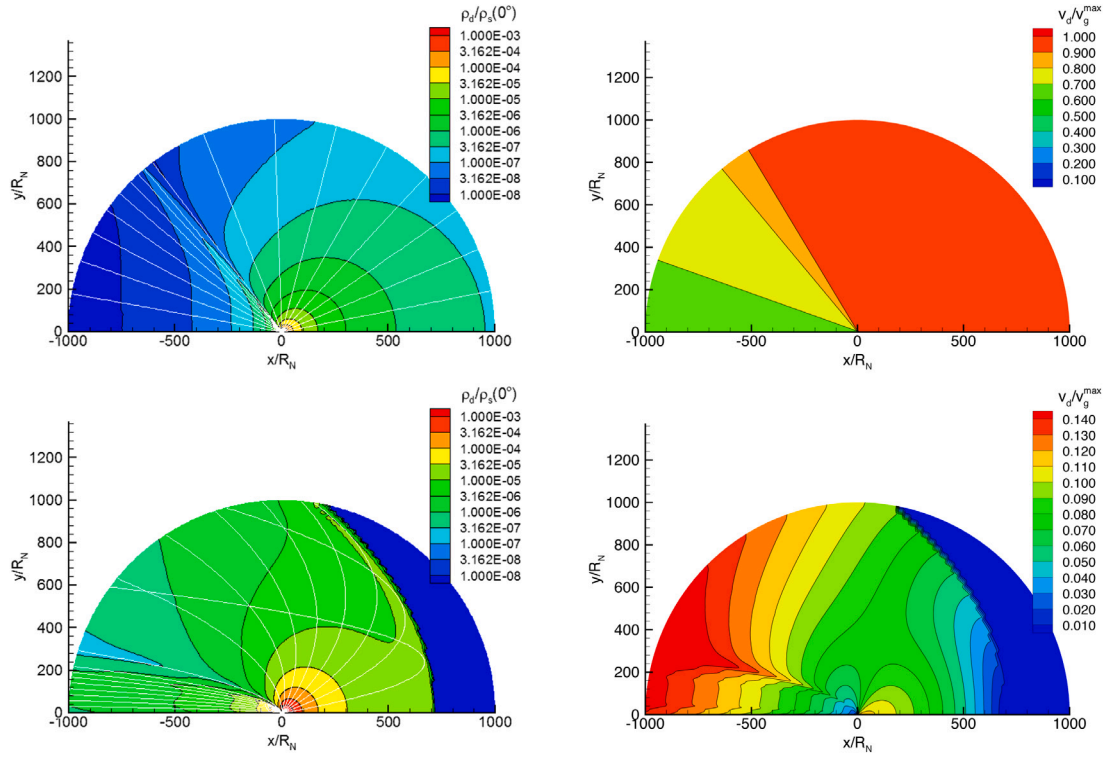

Fig. 3. Spatial distribution of dimensionless dust density $\rho_d/\rho_s(0°)$ (left) and velocity v_d/v_g^{max} (right) for the case Iv = 100, Fu = 10^{-9}, Ro = 10^{-7} (top line) and Iv = 10^{-2}, Fu = 10^{-9}, Ro = 10^{-5} (bottom line). White lines show the trajectories of dust grains. Gas distribution corresponds to the expansion from spherical source with surface flux $q \propto \max\{\cos(z_{sun}), 0.01\}$.

surface shifts closer to the nucleus with decreasing of Iv or increasing of Ro.

Fig. 4 shows the case when $q(z_{sun}) = const$, i.e. the gas expansion is perfectly spherical (see Fig. 1 top panels) and therefore, beyond the region of strong acceleration, the gas drag decreases at the same rate as the gravitational attraction by the nucleus. In this case the influence of gravity (characterized by Fu) is practically undetectable (lines with different pattern and symbols with different shape overlap each other) in the whole range of parameters variation when Iv > 10^{-3}. When the turning surface is located closer than $r/R_N = 100$ or 1000 this results in an abrupt drop to zero of the angular distribution of normalized density (at corresponding r/R_N).

In the cases shown in Figs. 5–7 the gas emission occurs mostly from the day-side. The gas from the day-side expands into the night-side, where it interacts with the gas emitted from the night side and forms shock structures (qualitatively similar to bottom panels in Fig. 1). This causes non-monotonic angular variation of the normalized dust density at $z_{sun} > 90°$. On the night side ($z_{sun} > 90°$), the angular distribution of the normalized dust density becomes more sensitive to the variation of Ro and Fu, with decreasing of Iv.

It can be clearly seen in Figs. 4–7 that for a given Iv $\geq 10^{-3}$ the angular distributions of the normalized dust density at $r/R_N = 100$ and 1000 have close values for $0° \leq z_{sun} \leq 100°$ in a broad range of parameters Fu and Ro. This part of the angular distribution of the normalized dust density we will call the *general profile* (it is shown by black line with black circles in Figs. 4–7). For Iv < 10^{-3} the general profile at $r/R_N = 100$ and 1000 is absent since the turning surface is closer than $r/R_N = 1000$ for all considered Fu and Ro.

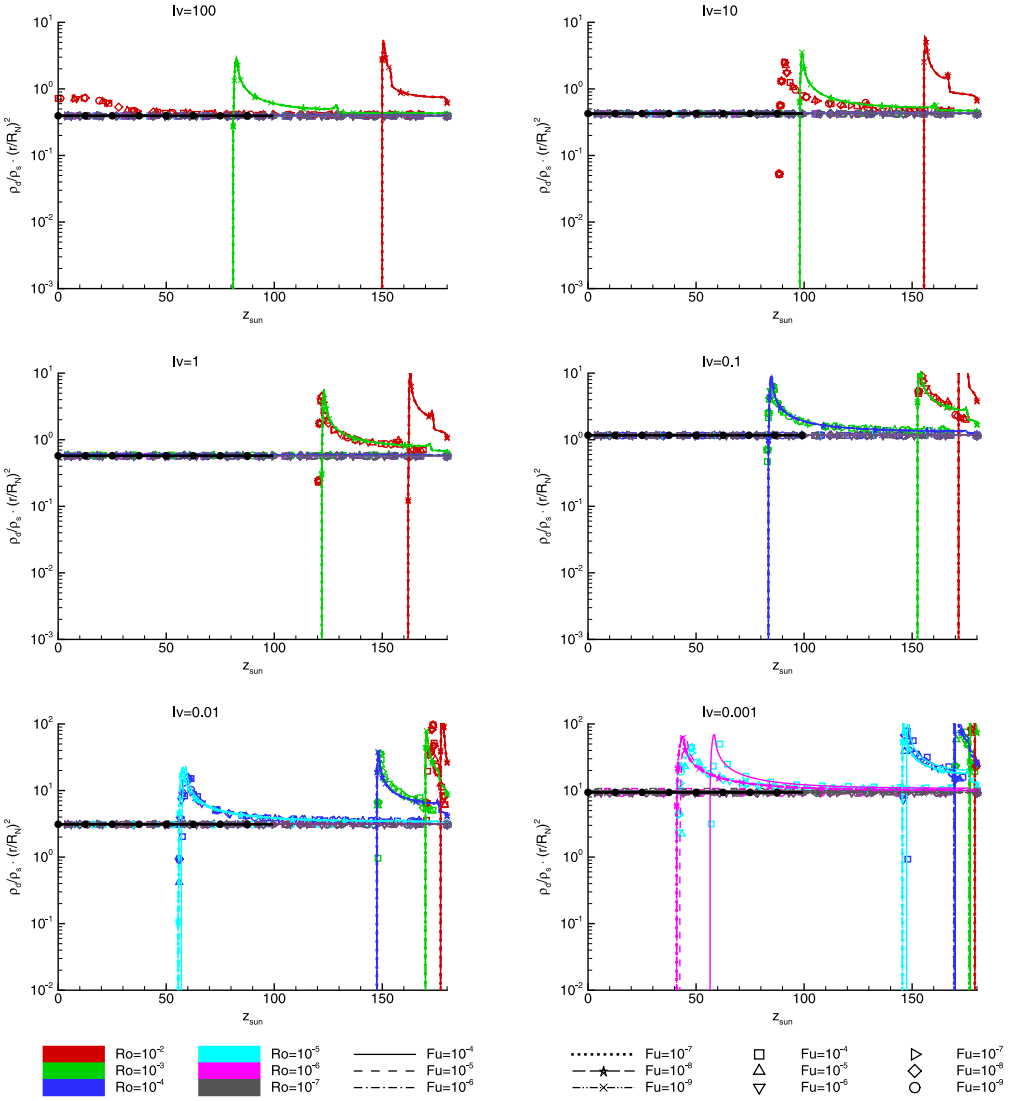

Fig. 4. Angular distribution of the normalized dust density $\rho_d/\rho_s \cdot (r/R_N)^2$ at $r/R_N = 100$ (symbols) and 1000 (lines). Gas distribution corresponds to the expansion from a spherical nucleus with surface flux $q(z_{sun}) = const$. Each panel corresponds to a specific value of Iv ($10^{-3} \le$ Iv $\le 10^2$): Iv = 100 (top left), Iv = 10 (top right), Iv = 1 (second line left), Iv = 0.1 (second line right), Iv = 10^{-2} (third line left), Iv = 10^{-3} (third line right). The color of the lines and symbols corresponds to different values of Ro ($10^{-7} \le$ Ro $\le 10^{-2}$). The shape of symbols and pattern of the line correspond to different values of Fu ($10^{-9} \le$ Fu $\le 10^{-4}$).

It is possible to fit the general profiles shown in Figs. 4–7 with a polynomial function of the kind:

$$\frac{\rho_d(z_{sun})}{\rho_s(0°)}\left(\frac{r}{R_N}\right)^2 = a_0 + a_1\cos(z_{sun}) + a_2\cos^2(z_{sun}) \quad (24)$$

where a_i values are reported in Table 2. The coefficients in Table 2 were derived by least-squares fitting of Eq. (24) to the general profile shown in Figs. 4–7 (black lines with black circles) in the range $0° \le z_{sun} \le 100°$. We remind that the fitting corresponds to the dust-to-gas mass flux ratio $\chi = 1$.

3.3. Approximation of the dust density along the sun–comet line

In the paraxial region, the gas flow is close to spherical expansion. Therefore, we may expect that in some conditions (combinations of Iv, Fu, Ro) the dust flow in this region can be close to the flow from a spherical source. If the velocity is constant, the density varies proportionally to r^{-2}. We define the relative variation of the dust density Δ_ρ in the region $100 \le r/R_N \le 1000$:

$$\Delta_\rho = 2 \cdot \frac{|\rho_d(r/R_N = 100) - \rho_d(r/R_N = 1000) \cdot 10^2|}{\rho_d(r/R_N = 100) + \rho_d(r/R_N = 1000) \cdot 10^2} \quad (25)$$

Fig. 8 shows isosurface of $\Delta_\rho = 0.1$ in the Iv, Fu, Ro parameter space for two cases of gas production: (1) $\alpha = 1$ and $a_n = 1.0$ i.e. spherical expansion of the gas; and (2) $\alpha = 1$ and $a_n = 0.01$. For Ro beyond the space covered by the isosurface $\Delta_v = 0.1$, the distribution of dust density in the region $100 < r/R_N < 1000$ does not follow "r^{-2}" law. The isosurfaces of Δ_ρ for the cases of gas production with $\alpha > 1$ are very similar to the ones shown in Fig. 8, therefore we do not show them.

Fig. 9 shows the distribution of $\rho_d/\rho_s \cdot (r/R_N)^2$ in the sunward direction. The variation of Fu in the range $10^{-9} \le$ Fu $\le 10^{-4}$ has a small effect on the dust density in the region $100 < r/R_N < 1000$ (the case with maximal Fu = 10^{-4} is shown by circles in Fig. 9). This is because two opposing forces, the gas drag and the nucleus attraction, are decreasing with the same rate in this region.

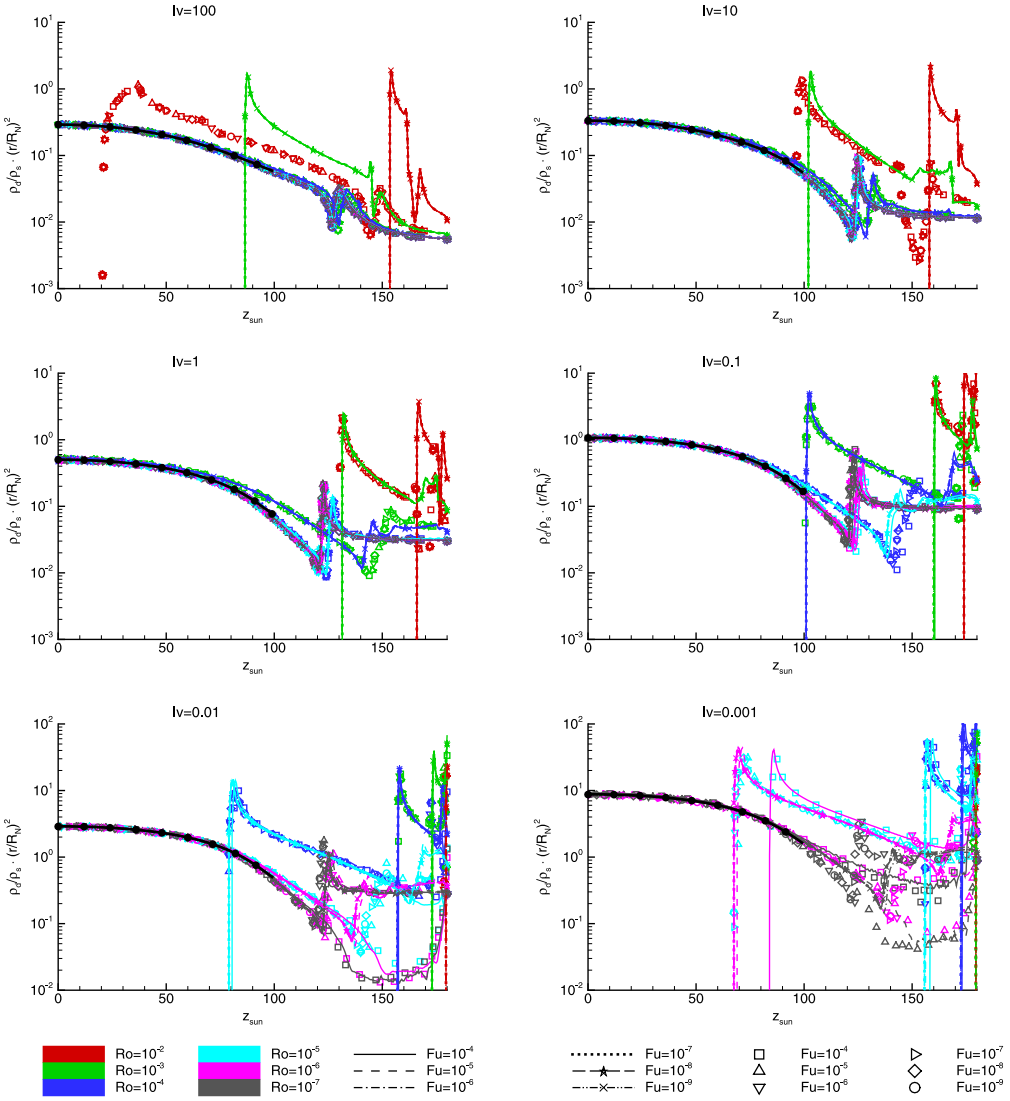

Fig. 5. Angular distribution of the normalized dust density $\rho_d/\rho_s \cdot (r/R_N)^2$ at $r/R_N = 100$ (symbols) and 1000 (lines). Gas distribution corresponds to the expansion from a spherical nucleus with surface flux $q(z_{sun}) \propto \max\{\cos(z_{sun}), 0.01\}$. Each panel corresponds to a specific value of Iv ($10^{-3} \le$ Iv $\le 10^{2}$): Iv = 100 (top left), Iv = 10 (top right), Iv = 1 (second line left), Iv = 0.1 (second line right), Iv = 10^{-2} (third line left), Iv = 10^{-3} (third line right). The color of the lines and symbols corresponds to different values of Ro ($10^{-7} \le$ Ro $\le 10^{-2}$). The shape of symbols and pattern of the line correspond to different values of Fu ($10^{-9} \le$ Fu $\le 10^{-4}$).

For the dust density at $100 \le x/R_N \le 1000$ along sunward direction for $10^{-4} <$ Iv ≤ 100 we propose the approximation:

$$\frac{\rho_d(z_{sun}=0°)}{\rho_s^0}\left(\frac{r}{R_N}\right)^2 = \sum_{i=0}^{i=n_i} c_i \cdot \{\log_{10}(\mathrm{Iv})\}^i \tag{26}$$

where c_i values are reported in Table 3. The coefficients of Table 3 were derived by least-squares fitting of Eq. (26) to the dust density at $x/R_N = 100$ shown in Fig. 10. This fitting corresponds to the dust-to-gas mass flux ratio $\chi = 1$.

We estimate the quality of the approximation by the relative difference ε of computed ("comp") and approximated ("approx") density:

$$\varepsilon = \frac{|\rho_{comp} - \rho_{approx}|}{\rho_{comp}}. \tag{27}$$

The approximation with coefficients values reported in Table 3 has a deviation of $\varepsilon < 0.11$.

4. Scaling of the terminal dust velocity

Introducing dimensionless parameters allows to determine a relationship between the parameters and to reveal a scaling law. For example, let us consider a spherical nucleus with uniform gas emission over the surface (i.e. $a_n = 1$) and, in addition, that the influence of the solar radiation pressure is negligible. These conditions correspond to the case studied in Zakharov et al. (2018). The numerical simulation of the dust terminal velocity in a wide range of parameters (Iv and Fu) shows (see Zakharov et al., 2018, fig.4) that at Iv < 0.1 and Fu < 0.01·Iv:

$$\frac{v_d(a)}{v_d(a_*)} = \sqrt{\frac{\mathrm{Iv}(a)}{\mathrm{Iv}(a_*)}}. \tag{28}$$

where a_* and $v_d(a_*)$ are the dust particle referential size and the corresponding terminal velocity, respectively. Therefore, the scaling

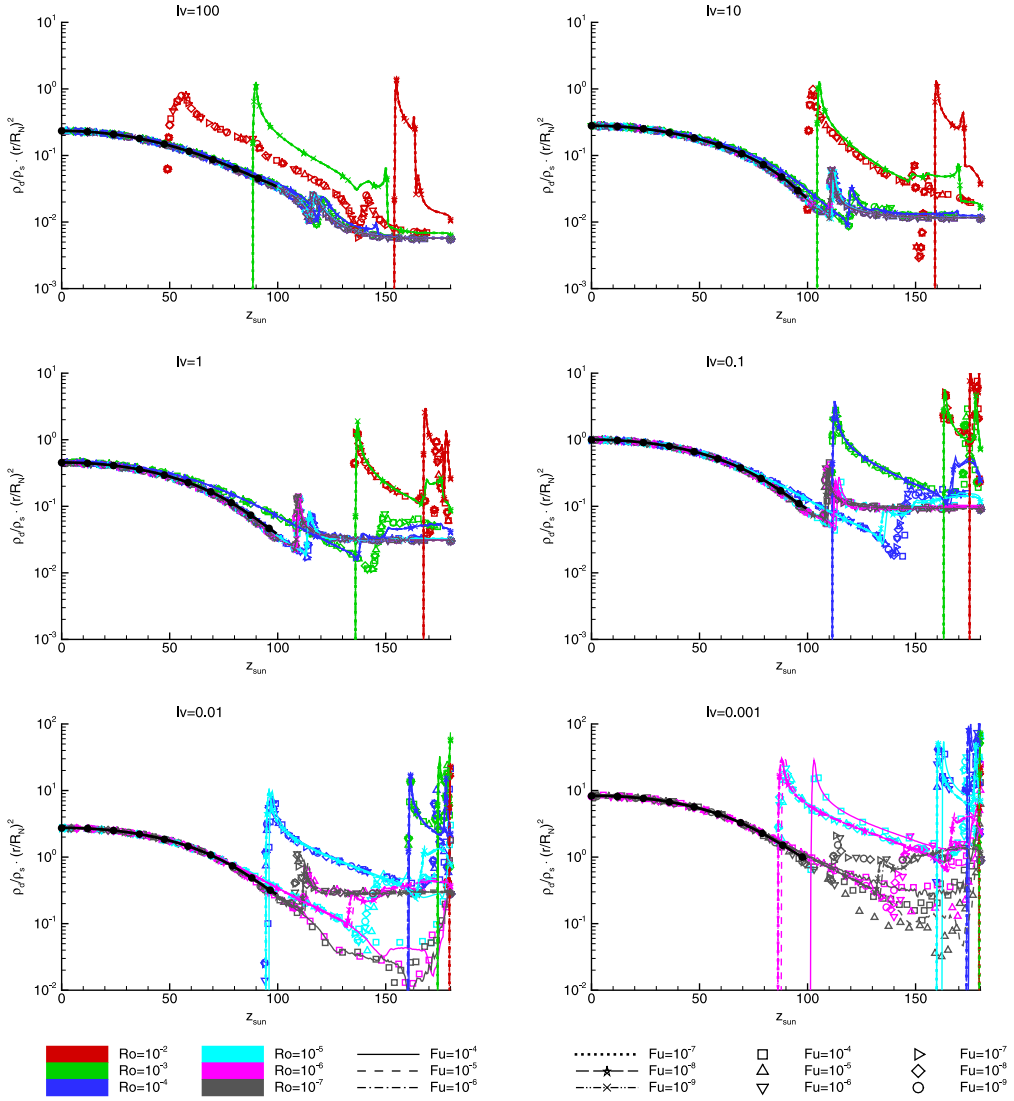

Fig. 6. Angular distribution of the normalized dust density $\rho_d/\rho_s \cdot (r/R_N)^2$ at $r/R_N = 100$ (symbols) and 1000 (lines). Gas distribution corresponds to the expansion from a spherical nucleus with surface flux $q(z_{sun}) \propto \max\{\cos^2(z_{sun}), 0.01\}$. Each panel corresponds to a specific value of Iv ($10^{-3} \le$ Iv $\le 10^2$): Iv = 100 (top left), Iv = 10 (top right), Iv = 1 (second line left), Iv = 0.1 (second line right), Iv = 10^{-2} (third line left), Iv = 10^{-3} (third line right). The color of the lines and symbols corresponds to different values of Ro ($10^{-7} \le$ Ro $\le 10^{-2}$). The shape of symbols and pattern of the line correspond to different values of Fu ($10^{-9} \le$ Fu $\le 10^{-4}$).

law for the dust particle terminal velocity is:

$$v_d \propto \sqrt{\frac{Q_g^{sph} m_g}{R_N a \varrho_d \sqrt{T_s/m_g}}}. \tag{29}$$

Partially, i.e. $v_d \propto f(Q_g, a, \varrho_d)$, this scaling law was empirically derived in Ivanovski et al. (2017) (equation 18), and later re-derived in Marschall et al. (2020)(equation 3, unfortunately, published with a typo!). The application of dimensionless parameters allows us to determine the relation for a larger set of factors (i.e. $v_d \propto f(Q_g, m_g, T_s, R_N, a, \varrho_d)$).

If the scaling is made for the same gas flow, then we arrive to the well known relation:

$$v_d \propto \frac{1}{\sqrt{a\varrho_d}}. \tag{30}$$

5. Conclusion

We have shown that the proposed dimensionless parameters allow us to scale available coma dust distributions. This allows us to reduce the number of cases to be investigated in a comprehensive study. The approach that considers the variation of a large number of physical parameters can be replaced with a new approach that considers a limited number of dimensionless parameters, i.e. generalized parameters. When parameters of the flow are known with large uncertainty it is necessary to make multiple simulations, varying each of parameters in some range, using generalized parameters allows us to reduce greatly the parameter space.

We propose approximations for the angular variation of dust density and for the dust density along sunward direction, for the following ranges of generalized parameters: $10^{-7} \le$ Iv $\le 10^2$, $10^{-9} \le$ Fu $\le 10^{-4}$, $10^{-7} \le$ Ro $\le 10^{-2}$ (i.e. $10^{-3} \le$ Ro/Fu $\le 10^7$).

It is important to note, that the scaling does not depend on the model of gas flow (i.e. how the gas distribution was obtained – via numerical integration of Euler or Navier–Stokes equations, or the direct simulation Monte-Carlo). However, it should be noted that if, for scaling, it is necessary to change the characteristic size and/or gas production, only the gas flow description based on the Euler equations remains physically consistent.

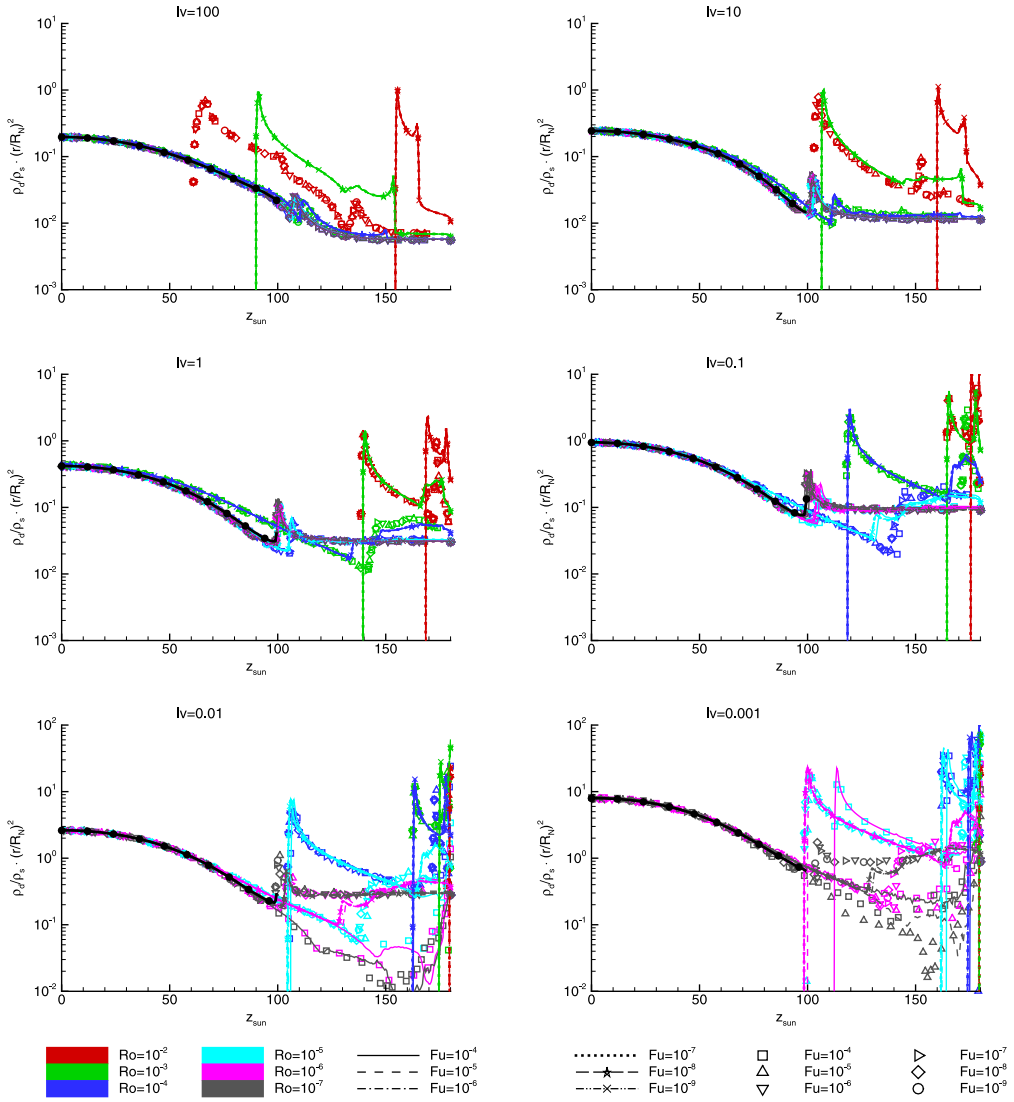

Fig. 7. Angular distribution of the normalized dust density $\rho_d/\rho_s \cdot (r/R_N)^2$ at $r/R_N = 100$ (symbols) and 1000 (lines). Gas distribution corresponds to the expansion from a spherical nucleus with surface flux $q(z_{sun}) \propto \max\{\cos^3(z_{sun}), 0.01\}$. Each panel corresponds to a specific value of Iv ($10^{-3} \le$ Iv $\le 10^2$): Iv = 100 (top left), Iv = 10 (top right), Iv = 1 (second line left), Iv = 0.1 (second line right), Iv = 10^{-2} (third line left), Iv = 10^{-3} (third line right). The color of the lines and symbols corresponds to different values of Ro ($10^{-7} \le$ Ro $\le 10^{-2}$). The shape of symbols and pattern of the line correspond to different values of Fu ($10^{-9} \le$ Fu $\le 10^{-4}$).

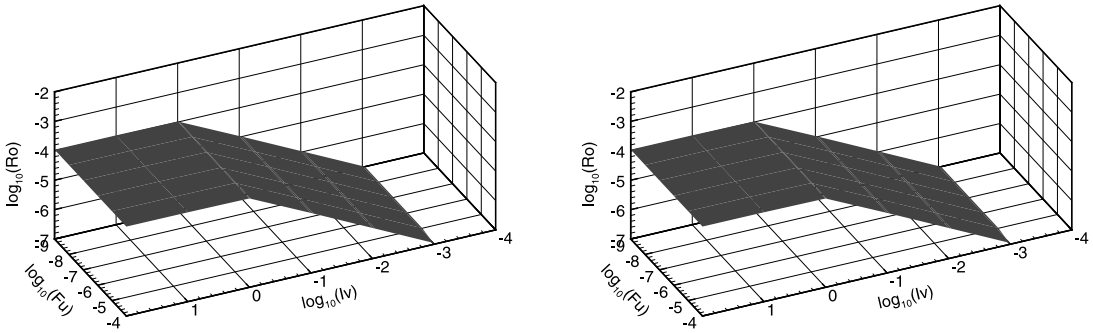

Fig. 8. Isosurface of $\Delta_\rho = 0.1$ in the parameter space Iv, Fu, Ro. The gas distribution corresponds to the spherical expansion (left) and the expansion form a spherical nucleus with surface gas production $q(z_{sun}) \propto \max\{\cos(z_{sun}), 0.01\}$.

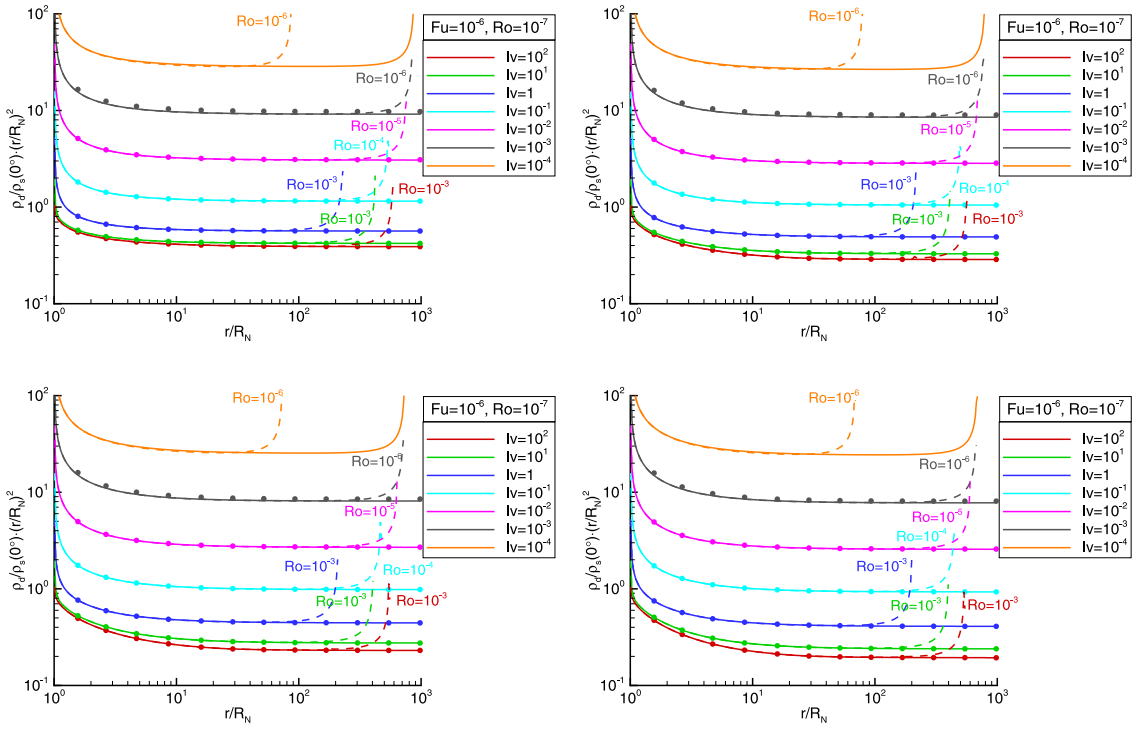

Fig. 9. The distribution of $\rho_d/\rho_s(0^\circ)\cdot(r/R_N)^2$ in the sunward direction. Solid lines correspond to Fu = 10^{-6}, Ro = 10^{-7}; circles correspond to Fu = 10^{-4}, Ro = 10^{-7}; dashed lines correspond to Fu = 10^{-6} and Ro > 10^{-7}. The gas distribution corresponds to the expansion form a spherical nucleus with surface gas production $q(z_{sun}) \propto \max(\cos^{\alpha}(z_{sun}), a_n)$: $\alpha = 1$ and $a_n = 1.0$ (top left), $\alpha = 1$ and $a_n = 0.01$ (top right), $\alpha = 2$ and $a_n = 0.01$ (bottom left), $\alpha = 3$ and $a_n = 0.01$ (bottom right).

Table 2
Coefficients for approximation of angular distribution of dust density (Eq. (24)).

Iv	Fu	Ro	a_0	a_1	a_2
$q \propto \max\{\cos^1(z_{sun}), 1.0\}$					
10^2	$10^{-9} \le$ Fu $\le 10^{-4}$	$10^{-7} \le$ Ro $\le 10^{-4}$	0.3949	0.000	0.000
10^1	$10^{-9} \le$ Fu $\le 10^{-4}$	$10^{-7} \le$ Ro $\le 10^{-4}$	0.4264	0.000	0.000
10^0	$10^{-9} \le$ Fu $\le 10^{-4}$	$10^{-7} \le$ Ro $\le 10^{-4}$	0.5734	0.000	0.001
10^{-1}	$10^{-9} \le$ Fu $\le 10^{-4}$	$10^{-7} \le$ Ro $\le 10^{-5}$	1.167	0.000	0.000
10^{-2}	$10^{-9} \le$ Fu $\le 10^{-4}$	$10^{-7} \le$ Ro $\le 10^{-5}$	3.112	−0.002	0.001
10^{-3}	$10^{-9} \le$ Fu $\le 10^{-4}$	$10^{-7} \le$ Ro $\le 10^{-6}$	9.380	−0.009	0.003
$q \propto \max\{\cos^1(z_{sun}), 0.01\}$					
10^2	$10^{-9} \le$ Fu $\le 10^{-4}$	$10^{-7} \le$ Ro $\le 10^{-4}$	0.07790	0.1409	0.07299
10^1	$10^{-9} \le$ Fu $\le 10^{-4}$	$10^{-7} \le$ Ro $\le 10^{-4}$	0.08764	0.2105	0.03546
10^0	$10^{-9} \le$ Fu $\le 10^{-4}$	$10^{-7} \le$ Ro $\le 10^{-4}$	0.1271	0.3803	−0.004260
10^{-1}	$10^{-9} \le$ Fu $\le 10^{-4}$	$10^{-7} \le$ Ro $\le 10^{-5}$	0.2829	0.9015	−0.1129
10^{-2}	$10^{-9} \le$ Fu $\le 10^{-4}$	$10^{-7} \le$ Ro $\le 10^{-5}$	0.8034	2.545	−0.4452
10^{-3}	$10^{-9} \le$ Fu $\le 10^{-4}$	$10^{-7} \le$ Ro $\le 10^{-6}$	2.565	7.335	−1.082
$q \propto \max\{\cos^2(z_{sun}), 0.01\}$					
10^2	$10^{-9} \le$ Fu $\le 10^{-4}$	$10^{-7} \le$ Ro $\le 10^{-4}$	4.606	0.07924	0.1080
10^1	$10^{-9} \le$ Fu $\le 10^{-4}$	$10^{-7} \le$ Ro $\le 10^{-4}$	4.322	0.1467	0.08967
10^0	$10^{-9} \le$ Fu $\le 10^{-4}$	$10^{-7} \le$ Ro $\le 10^{-4}$	6.534	0.2224	0.1687
10^{-1}	$10^{-9} \le$ Fu $\le 10^{-4}$	$10^{-7} \le$ Ro $\le 10^{-5}$	0.1484	0.5395	0.3194
10^{-2}	$10^{-9} \le$ Fu $\le 10^{-4}$	$10^{-7} \le$ Ro $\le 10^{-5}$	0.4214	1.585	0.7617
10^{-3}	$10^{-9} \le$ Fu $\le 10^{-4}$	$10^{-7} \le$ Ro $\le 10^{-6}$	1.380	4.406	2.665
$q \propto \max\{\cos^3(z_{sun}), 0.01\}$					
10^2	$10^{-9} \le$ Fu $\le 10^{-4}$	$10^{-7} \le$ Ro $\le 10^{-4}$	0.03186	0.05034	0.1133
10^1	$10^{-9} \le$ Fu $\le 10^{-4}$	$10^{-7} \le$ Ro $\le 10^{-4}$	0.02536	0.09747	0.1206
10^0	$10^{-9} \le$ Fu $\le 10^{-4}$	$10^{-7} \le$ Ro $\le 10^{-4}$	0.04089	0.1085	0.2705
10^{-1}	$10^{-9} \le$ Fu $\le 10^{-4}$	$10^{-7} \le$ Ro $\le 10^{-5}$	0.09761	0.2431	0.6087
10^{-2}	$10^{-9} \le$ Fu $\le 10^{-4}$	$10^{-7} \le$ Ro $\le 10^{-5}$	0.2847	0.7420	1.604
10^{-3}	$10^{-9} \le$ Fu $\le 10^{-4}$	$10^{-7} \le$ Ro $\le 10^{-6}$	0.9060	2.127	4.989

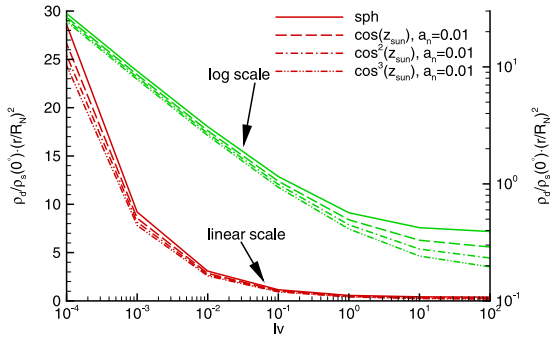

Fig. 10. Dust density $\rho_d/\rho_s(0^\circ)\cdot(r/R_N)^2$ at $x/R_N = 100$. The gas distribution corresponds to the expansion form a spherical nucleus with a uniform gas production i.e. $q(z_{sun}) = const$ ("sph"), and a surface gas production $q(z_{sun}) \propto \max(\cos^{\alpha}(z_{sun}), 0.01)$ and $1 \le \alpha \le 3$.

Table 3
Coefficients for approximation (n_i=4) of dust density (Eq. (26)) along sunward direction for the case of gas production $q(z_{sun}) \propto \max(\cos^{\alpha}(z_{sun}), a_n)$.

α	a_n	c_0	c_1	c_2	c_3	c_4
1.0	1.00	0.5971	−0.1922	0.08239	−0.1301	0.05575
1.0	0.01	0.5188	−0.2007	0.07265	−0.1195	0.05237
2.0	0.01	0.4693	−0.2025	0.06954	−0.1134	0.04990
3.0	0.01	0.4315	−0.2000	0.06731	−0.1086	0.04776

It is possible to extend the scope of processes for scaling (i.e. rotation of grains Ivanovski et al., 2017) by introducing the additional dimensionless parameters in the same manner.

Acknowledgments

This research was supported by the Italian Space Agency (ASI) within the ASI-INAF agreements I/032/05/0, I/024/12/0 and 2020-4-HH.0, and by Peter the Great St.Petersburg Polytechnic University (Ministry of Education and Science of the Russian Federation).

References

Bird, G.A., 1994. Molecular Gas Dynamics and the Direct Simulation of Gas Flows. Clarendon Press, Oxford.

Crifo, J.-F., Loukianov, G.A., Rodionov, A.V., Zakharov, V.V., 2005. Direct Monte Carlo and multifluid modeling of the circumnuclear dust coma. Spherical Grain Dyn. Rev. Icarus 176 (1), 192–219.

Crifo, J.-F., Lukianov, G.A., Rodionov, A.V., Khanlarov, G.O., Zakharov, V.V., 2002. Comparison between Navier–Stokes and direct Monte-Carlo simulations of the circumnuclear coma. I. Homogeneous, spherical source. Icarus 156, 249–268.

Crifo, J.-F., Rodionov, A.V., 1997. The dependence of the circumnuclear structure on the properties of the nucleus. I. Comparison between a homogeneous and an inhomogeneous spherical nucleus, with application to Comet P/Wirtanen. Icarus 127, 319–353.

Fougere, N., Combi, M.R., Rubin, M., Tenishev, V., 2013. Modeling the heterogeneous ice and gas coma of Comet 103P/Hartley 2. Icarus 225, 688–702.

Fulle, M., 2004. In: Festou, M.C., Keller, H.U., Weaver, H.A. (Eds.), Motion of Cometary Dust, Comets II, Vol. 745. University of Arizona Press, Tucson, pp. 565–575.

Fulle, M., Colangeli, L., Mennella, V., Rotundi, A., Bussoletti, E., 1995. The sensitivity of the size distribution to the grain dynamics: simulation of the dust flux measured by GIOTTO at P/Halley. Astron. Astrophys. 304 (622).

Gombosi, T.I., Nagy, A.F., Cravens, T.E., 1986. Dust and neutral gas modeling of the inner atmospheres of comets. Rev. Geophys. 24, 667–700.

Ivanovski, S.L., Zakharov, V.V., Della Corte, V., Crifo, J.-F., Rotundi, A., Fulle, M., 2017. Dynamics of aspherical dust grains in a cometary atmosphere: I. axially symmetric grains in a spherically symmetric atmosphere. Icarus 282, 333–350. http://dx.doi.org/10.1016/j.icarus.2016.09.024.

Landau, L.D., Lifshitz, E.M., 1976. Mechanics, third ed. Pergamon Press, Oxford.

Marschall, R., Markkanen, J., Gerig, S.-B., Pinzón-Rodríguez, O., Thomas, N., Wu, J.-S., 2020. The dust-to-gas ratio, size distribution, and dust fall-back fraction of comet 67P/Churyumov-Gerasimenko: Inferences from linking the optical and dynamical properties of the inner comae. Frontiers in Physics 8, 227. http://dx.doi.org/10.3389/fphy.2020.00227.

Marschall, R., Su, C.C., Liao, Y., Thomas, N., Altwegg, K., Sierks, H., Ip, W.-H., Keller, H.U., Knollenberg, J., Kuhrt, E., Lai, I.L., Rubin, M., Skorov, Y., Wu, J.S., Jorda, L., Preusker, F., Scholten, F., Gracia-Berna, A., Gicquel, A., Naletto, G., Shi, X., Vincent, J.-B., 2016. Modelling observations of the inner gas and dust coma of comet 67P/Churyumov-Gerasimenko using ROSINA/COPS and OSIRIS data: First results. Astron. Astrophys. 589 (17), id.A90.

Probstein, R.F., 1969. The dusty gas dynamics of comet heads. In: Lavrent'ev, M.A. (Ed.), Problems of Hydrodynamics and Continuum Mechanics. SIAM, Philadelphia, pp. 568–583.

Rodionov, A.V., Crifo, J.-F., Szego, K., Lagerros, J., Fulle, M., 2002. An advanced physical model of cometary activity. Planet. Space Sci. 50 (10–11), 983–1024.

Snodgrass, C., Jones, G.H., 2019. The European space agency's comet interceptor lies in wait. Nature Commun. 10, 5418. http://dx.doi.org/10.1038/s41467-019-13470-1, id.

Tenishev, V., Combi, M.R., Rubin, M., 2011. Numerical simulation of dust in a cometary coma: Application to comet 67P/Churyumov–Gerasimenko. Astrophys. J. 732 (104).

Whipple, F.S., 1950. A comet model. II. Physical relations for comets and meteors. Agron. J. 111, 464–474.

Zakharov, V.V., Ivanovski, S.L., Crifo, J.-F., Della Corte, V., Rotundi, A., Fulle, M., 2018. Asymptotics for spherical particle motion in a spherically expanding flow. Icarus 312, 121–127.

Zakharov, V.V., Rodionov, A.V., Fulle, M., Ivanovski, S.L., Bykov, N.Y., Della Corte, V., Rotundi, A., 2021. Practical relations for assessments of the gas coma parameters. Icarus 354, 114091. http://dx.doi.org/10.1016/j.icarus.2020.114091.

Zakharov, V.V., Rodionov, A.V., Lukianov, G.A., Crifo, J.F., 2009. Monte-Carlo and multifluid modelling of the circumnuclear dust coma II. Aspherical-homogeneous, and spherical-inhomogeneous nuclei. Icarus 201 (1), 358–380.